ChemElectroChem

Research Article
doi.org/10.1002/celc.202500121

Chemistry Europe
European Chemical Societies Publishing

www.chemelectrochem.org

Surface Acidity of Basic Oxides: The Case Study of Solvated ZnO from Density Functional Theory-Based Molecular Dynamics Simulations

Aishwarya Sudhama and Chao Zhang*

Zinc oxide is a versatile semiconducting metal oxide for both environmental and energy applications. Here, the surface acidity of the ZnO($10\bar{1}0$)/NaCl sol. system is investigated by applying density functional theory-based molecular dynamics simulations. A new set of repulsive potential is developed, which leads to a consistent description of pK_a of $Zn_2O_sH^+$. By exploring the relation between the vertical energy gap at the deprotonated state (of acid) and the corresponding pK_a, this work reveals that different sets of repulsive potentials are likely needed for accurate predictions of surface acidity for basic oxides.

1. Introduction

The structure and dynamics of water on nonpolar ZnO ($10\bar{1}0$) surface has been extensively investigated in various experimental[1,2] and theoretical works,[3–7] owing to its widespread relevance in heterogenous catalysis, water splitting photocatalysis,[8] and pH-dependent solubility and toxicity.[9]

Water can rapidly dissociate and recombine on this surface, triggered by various proton transfer (PT) mechanisms. Raymand et al.[3] have observed hydroxylation level from 50% (monolayer) to 80–85% (liquid water) in reactive force-field simulations. This increase was attributed to enhanced PT in the presence of liquid water. Tocci and Michaelides[5] have reported hydroxylation level of $55 \pm 5\%$ for liquid film using density functional theory-based molecular dynamics (DFTMD) simulations. They reveal that the increase in PT rate upon going from monolayer coverage to liquid multilayer is due to specific solvent-induced fluctuations in the H-bond network which decreases PT barriers as well as activates alternate PT mechanisms within the contact layer. Such PT mechanisms have also been observed by Kharche et al.[4] The structural and dynamical properties of various interfacial species were then extensively investigated by Quaranta et al.[6] using reactive molecular dynamics simulations using neural network potential. They reported average surface hydroxylation level of 71%. They characterized the two types of PT reactions as surface PT and adlayer PT, with adlayer PT rate significantly larger. They also emphasize on the importance of hydrogen bond fluctuations ("presolvation") as a necessary factor governing the rate of PT and, consequently, water dissociation. The group further investigated even slow events such as water exchange between the surface and the bulk liquid and also PT lifetimes.[7] They analyzed and characterized the structural motifs in great detail. They showed that the adsorbed OH^- ions are always bound to a single Zn site and never bridges two surface Zn ions. They further showed that a greater proportion of adsorbed water molecules are pointing towards the surface, that is, in an "H-down" configuration.

When ZnO ($10\bar{1}0$) surface is in contact with aqueous solution, two types of surface active species can be encountered depending on the pH of the solution.[10] The first is the adsorbed water on the terminal zinc site Zn_s, which can lose a proton to the aqueous solution and form negatively charged surface hydroxyl species Equation (1). The second is the positively charged surface hydroxyl species formed by protonation of the surface bridging oxygen O_s Equation (2).

$$Zn_sOH_2 \rightleftharpoons Zn_sOH^- + H^+(aq), K_{a1} \quad (1)$$

$$Zn_2O_sH^+ \rightleftharpoons Zn_2O_s + H^+(aq), K_{a2} \quad (2)$$

Using this two-site model, the relation between the acidities of the surface groups (pK_a), point of zero net proton charge (PZC), and water dissociation free energy ($\Delta A_{diss,H_2O}$) can be established as follows.

$$PZC = \frac{1}{2}(pK_{a1} + pK_{a2}) \quad (3)$$

$$\Delta A_{diss,H_2O} = 2.3k_BT(pK_{a1} - pK_{a2}) \quad (4)$$

In this work, we have applied DFTMD simulations and the free energy perturbation method to compute the pK_a's of surface hydroxyls formed on the ZnO ($10\bar{1}0$)/NaCl sol. interface. Through reparameterization of the so-called repulsive potential V_{rep}, we show that the optimized repulsive potential leads to a consistent description of pK_a of $Zn_2O_sH^+$. It further allows us to establish a relationship between the vertical energy gap

A. Sudhama, C. Zhang
Department of Chemistry-Ångström Laboratory
Uppsala University
Lägerhyddsvägen 1, BOX 538, 75121 Uppsala, Sweden
E-mail: chao.zhang@kemi.uu.se

Supporting information for this article is available on the WWW under https://doi.org/10.1002/celc.202500121

$\langle \Delta E \rangle_1$ at the deprotonated state and the surface pK_a value. These insights suggest that different V_{rep} are needed to provide accurate prediction of surface acidity for ZnO.

2. Theory and Methods

2.1. Deprotonation Free Energy and Free Energy Perturbation

DFTMD implementation of the free energy perturbation method[11,12] can be used to compute the deprotonation free energy (therefore the pK_a) for a generic acid AH according to Equation (5).

$$AH(aq) \rightarrow A^-(aq) + H^+(aq) \quad (5)$$

Using free energy perturbation method, the deprotonation free energy $\Delta_{dp} A$ can be estimated as the time average of vertical deprotonation energy gap $\langle \Delta E \rangle_\lambda$ for insertion (or removal) of protons in a system controlled by a mapping potential for a sufficiently long MD trajectory run, where

$$\langle \Delta E \rangle_\lambda = \langle E_{A^-} \rangle_\lambda - \langle E_{AH} \rangle_\lambda \quad (6)$$

The mapping potential energy E_λ is a linear function of the coupling parameter λ, which connects the potential energy surface of the two end states AH and A^-.

$$E_\lambda = (1-\lambda)E_{AH} + \lambda E_{A^-} + V_{rd} \quad (7)$$

For given λ, vertical deprotonation energy $\langle \Delta E \rangle_\lambda$ is calculated by switching off the charge of the acid proton, transforming it instantaneously into a "dummy" or "ghost" atom which has no coulombic interactions with the electrons and nuclei in the system. To ensure reversible (de)protonation, this dummy atom is subject to a restraining harmonic potential V_{rd} which serves two purposes. In the protonated limit, it prevents strong acids to dissociate during the simulation run. In the deprotonated limit, i.e., when the acid proton becomes a "dummy" or "ghost" atom, harmonic potential restraints maintain its equilibrium position close to where it was in the protonated state.

Integration of $\langle \Delta E \rangle_\lambda$ over the coupling parameter λ from 0 to 1 gives the deprotonation free energy

$$\Delta_{dp} A = \int_0^1 d\lambda \langle \Delta E \rangle_\lambda \quad (8)$$

In practice, numerical integration of Equation (8) is normally carried out using Simpson's rule.

2.2. pK_a and Full Reaction Schemes

As explained by Cheng, Sprik, and colleagues,[11,12] the practical computation of pK_a in condensed phase systems under periodic boundary conditions (PBCs) needs special care. For the half reaction scheme considering the insertion/deletion of a single proton in the simulation cell, the reference (zero) of the electrostatic potential in simulations using PBCs is arbitrary and has no physical meaning. This bias in reference cancels out when one uses a full reaction scheme where deprotonation of a species/group is carried out in conjunction with protonation of another species in the same cell, avoiding a change of net charge. The full reaction scheme further enjoys the benefit of error cancellation in zero-point energy. In this study, two full reactions 9 and 10 are considered and the respective model systems are shown in **Figure 1**.

$$Zn_sOH^- + H_2O(aq) \rightarrow Zn_sOH_2 + OH^-(aq), \Delta A_1 \quad (9)$$

$$Zn_2O_sH^+ + H_2O(aq) \rightarrow Zn_2O_s + H_3O^+(aq), \Delta A_2 \quad (10)$$

This leads to the estimate of the pK_a of $ZnOH_2$ and Zn_2OH^+ respectively as

$$pK_{a1} = pK_{a,H_2O} - \frac{\Delta A_1}{2.3 k_B T} \quad (11)$$

$$pK_{a2} = pK_{a,H_3O^+} + \frac{\Delta A_2}{2.3 k_B T} \quad (12)$$

For simplicity, we have used the experimental value for the dissociation constant of water, i.e., $pK_w = 14.0$. Thus, the corresponding references are $pK_{a,H_3O^+} = -1.74$ and $pK_{a,H_2O} = 15.74$.

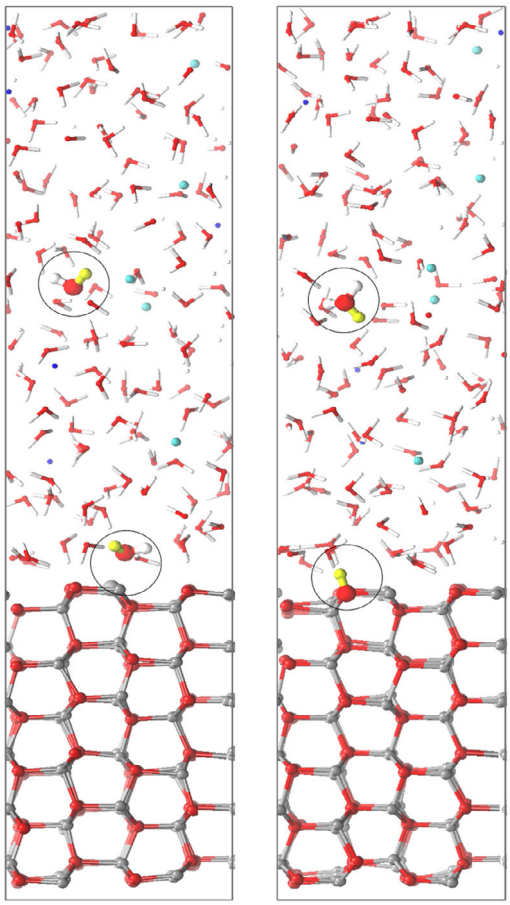

Figure 1. Illustrations of the ZnO(10$\bar{1}$0)/NaCl sol. system used in this study. The atoms represented in yellow color are the "dummy" atoms. The circles highlight the groups involved in the full reaction schemes shown in Equation (9) and (10).

2.3. Restraining and Repulsive Potentials

In practical simulations of pK_a, additional considerations need to be taken. A common practice[13] is to introduce a restraining potential into the mapping potential as

$$E_\lambda = (1-\lambda)E_{AH} + \lambda E_{A^-} + V_{rd} + V_{rH} \quad (13)$$

The notation V_{rH} in Equation (13) implies that the restraining potentials are applied to all the O-H bonds of the solvent water molecules, avoiding water dissociation and PT events. This restraint eliminates the possibility of reprotonation of the deprotonated site during the DFTMD simulation and improves the simulation stability.

For interfacial systems which show a high degree of water dissociation, an alternative scheme has been proposed recently. Jia et al.[14] introduced a Buckingham-type repulsive potential V_{rep} and applied it between the deprotonated site and all other neighboring hydrogens of solvent water molecules to prevent protonation of that site. Therefore, the mapping potential energy becomes

$$E_\lambda = (1-\lambda)E_{AH} + \lambda(E_{A^-} + V_{rep}) + V_{rd} \quad (14)$$

This allows reversible water dissociation on the surface of metal oxide to happen spontaneously, which is preferable to the case of ZnO. It is worth noting that V_{rep} only applies to the deprotonated state because V_{rep} should be zero for the protonated state (see Figure S2, Supporting Information and the discussions around it in the Supporting Information).

2.4. Computational Setup

Figure 1 shows the simulation setup where the ZnO slab was constructed using a wurtzite unit cell with lattice parameters $a = 3.282$ Å, $c = 5.291$ Å, and orientation such that the z face which points towards the solution is non polar $(10\bar{1}0)$ surface. The unit cell is replicated as $4 \times 2 \times 3$ leading to a thickness of 6 layers. The electrolyte was initially equilibrated with classical MD which consists of 2 M solution of NaCl with 135 water molecules and 5 Na^+ and Cl^- ions each and placed on top of the ZnO Slab. The supercell has dimensions $13.128 \times 10.582 \times 47.054$ Å^3. For the pK_w calculations, cubic water box with $L = 9.86$ Å containing 32 water molecules were used.

To model the $Zn_2O_sH^+/Zn_2O_s$ species, a proton was placed near the bridging oxygen O_s of the ZnO Slab in its equilibrium configuration, and for the Zn_sOH_2/Zn_sOH^- species, a water molecule adsorbed to Zn_s of the ZnO slab was selected. All the DFTMD simulations have been performed using the CP2K program package.[15,16] The Becke exchange[17] and Lee-Yang-Parr[18] correlation (BLYP) functionals with TZV2P basis set for orbitals is used for H_2O. The Perdew–Burke–Ernzerhof (PBE) exchange-correlation functional,[19] DZVP in conjunction with molecular optimized (MOLOPT) basis sets was used for the ZnO/NaCl sol. interface.[20] Additionally, DFT-D3 dispersion corrections proposed by Grimme and coworkers[21] were included. The Goedecker–Teter–Hutter (GTH)[22,23] pseudopotentials have been used to represent the core electrons. The plane wave basis for the electron density was cutoff at 320 Ry. The target accuracy for the SCF convergence is 6.0×10^{-7} a.u. The time step for MD simulation is 0.5 fs, with the number of particles N, the volume V, and the temperature T kept constant (NVT ensemble). The target temperature of 330 K was imposed using Bussi–Donadio–Parrinello[24] thermostat. It is worth noting that for all the pK_as reported in this work, we assume the temperature to be 298 K, following the precedent.[25] The parameters for V_{rd} and V_{rH} are listed in Table S1, Supporting Information, and a summary of simulation length for the pK_a calculations is given in Table S3, Supporting Information, which can be found in the Supporting Information.

3. Results and Discussion

3.1. Reparametrization of the V_{rep} Scheme

The repulsive potential scheme introduced by Jia et al.[14] is of the form of Equation (15), where A has units of energy, B has units of length, and $r_{O^*-H_w}$ is the distance between the deprotonated site O^* to which dummy atom is attached and neighboring hydrogen atoms of solvent water molecules H_w. Parameters A and B need to be optimized so as to match the RDF $g_{O^*-H_w}(r)$ of the reference DFTMD simulation consisting of one OH^- in 31 water molecules with harmonic restraining potential V_{rH}.

$$V_{rep}(O^* - H_w) = A \cdot \exp\left(-\frac{r_{O^*-H_w}}{B}\right) \quad (15)$$

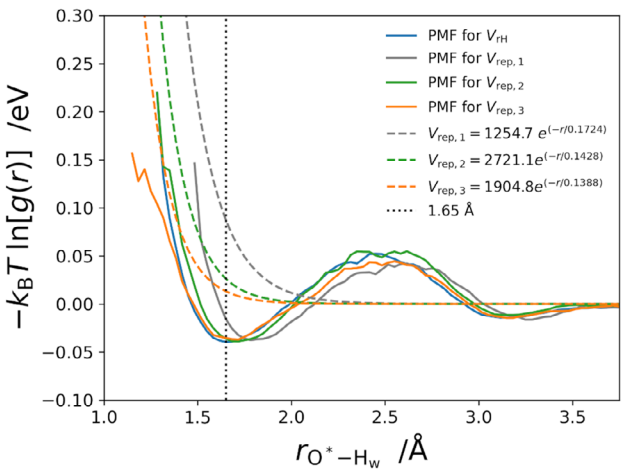

Figure 2. PMF curves (solid lines) between the O atom of OH^- and neighboring hydrogens of solvent water molecules H_w in a simulation box consisting of one OH^- in 31 water molecules. The blue curve represents the target PMF corresponding to the reference simulation with harmonic constraints V_{rH} for the same water box. The dotted black line represents the minimum of this curve, 1.65 Å. The dashed lines represents the variation of the potential $V_{rep} = A \cdot \exp^{(-r/B)}$ with for given A and B. $V_{rep,1}$, $V_{rep,2}$, $V_{rep,3}$ corresponds to parameters (1254.7 eV, 0.1724 Å), (2721.1 eV, 0.1428 Å), and (1904.8 eV, 0.1388 Å), represented by colors grey, green and orange respectively. The grey solid curve represents the PMF obtained using initial guess potential $V_{rep,1}$ as reported by Jia et al.[14] The green solid PMF curve is one of the intermediate step during optimization ($V_{rep,2}$). The orange solid PMF curve corresponds to the final optimized potential $V_{rep,3}$.

These parameters A and B were reported as 1254.7 eV and 0.1724 Å respectively in ref. [14]. Unfortunately, we found that using these parameters for similar simulation box of one OH^- in 31 water molecules lead to the radial distribution function (RDF) shift to the right as compared to that obtained from V_{rH} as the reference (see **Figure 2**). This meant that the solvation environment around OH^- with this V_{rep} is not optimal, with surrounding water molecules pushed farther away from OH^-.

Therefore, we have determined a new set of repulsive potential parameters in spirit of the iterative Boltzmann inversion.[26] The best parameters that we obtained are $A = 1904.77$ eV and $B = 0.1388$ Å. The corresponding potential of mean force (PMF), $-k_B T \ln g(r)$, is shown in Figure 2, which reproduces well with those obtained with reference V_{rH}.

We have further validated these parameters by computing the pK_w of liquid water system and comparing it to that obtained using harmonic restraining potential approach as the reference (See **Table 1**). $V_{rep,3}$ indeed leads to almost identical pK_w values as the one obtained using the restraining potential V_{rH}. Therefore, we have adopted $V_{rep,3}$ in the application shown in the next section.

Before closing up this part, it is worth noting that $r_{O^*-H_w}$ in Figure 2 and pK_w in Table 1 shows an interesting correlation: longer $O^* - H_w$ distance and higher pK_a value. We will revisit this observation and discuss it in light of the change in $\langle \Delta E \rangle_1$.

Table 1. The cumulative average of the vertical energy gaps, $\langle \Delta E \rangle_\lambda$, for $\lambda = 0, 0.5, 1$ during the simulation run of the half-reaction $H_2O(aq) \rightarrow OH^-(aq)$. Numerical integration using Simpson's rule was performed to estimate ΔA expressed in electron volts (eV). The pK_w was then determined using the reference deprotonation free energy $\Delta_{dp}A_{H_3O^+} = 15.35$ eV.

	A[eV], B[Å]	$\langle \Delta E \rangle_0$	$\langle \Delta E \rangle_{0.5}$	$\langle \Delta E \rangle_1$	ΔA [eV]	pK_w
$V_{rep,1}$	1254.7, 0.1724	18.388	16.667	14.022	16.513	16.37
$V_{rep,2}$	2721.1, 0.1428	18.361	16.643	13.467	16.400	14.46
$V_{rep,3}$	1904.8, 0.1388	18.345	16.583	13.309	16.331	13.31
V_{rH} (ref)		18.329	16.633	13.244	16.351	13.63

Table 2. Comparison between computed values for Zn_sOH_2 (pK_{a1}) and Zn_2OH^+ (pK_{a2}), PZC, and dissociation free energy $\Delta A_{diss,H_2O}$ [eV] for surface adsorbed water using the V_{rH} and V_{rep} schemes. V_{rep} here refers to $V_{rep,3}$ shown in Figure 2.

	pK_{a1}	pK_{a2}	PZC	$\Delta A_{diss,H_2O}$[eV]
V_{rH}	11.9	8.9/4.3	10.4/8.1	0.18/0.45
V_{rep}	8.6	5.7/5.1	7.1/6.9	0.17/0.21

3.2. Surface pK_as of the ZnO $(10\bar{1}0)$/NaCl Sol. System

The main results of surface pK_a of ZnO$(10\bar{1}0)$ using both the restraining potential and our optimized repulsive potential are shown in **Table 2**. For pK_a of Zn_sOH_2 (circles in **Figure 3**), introducing the repulsive potential V_{rep} lowers the corresponding value as compared to that obtained using the restraining potential V_{rH}. This is quite similar to what has been reported in the case of $SnO_2(110)/H_2O$ system and attributed to the electrostatic stabilization due to dissociated water.[14]

The results of pK_a for $Zn_2O_sH^+$, however, shows a distinction. Since the V_{rH} scheme does not allow solvent water molecules to dissociate on the ZnO$(10\bar{1}0)$ surface, the arrangement of water molecules on the slab surface remains highly structured, as illustrated in Figure 3.

Notably, water molecules exhibit two distinct modes of interaction with the alternate surface bridging oxygen sites. In the first configuration, water molecules (highlighted in yellow) orient such that their hydrogen atoms point directly toward the basic bridging oxygen. In contrast, at adjacent bridging oxygen sites, steric effects cause water molecules (cyan) to approach at an angle rather than directly. This alternating solvation pattern persists across the slab, influencing the acidity of the surface hydroxyl groups in distinct ways.

Considering the case where the surface hydroxyl interacts with a yellow water molecule, the RDF indicates that the distance

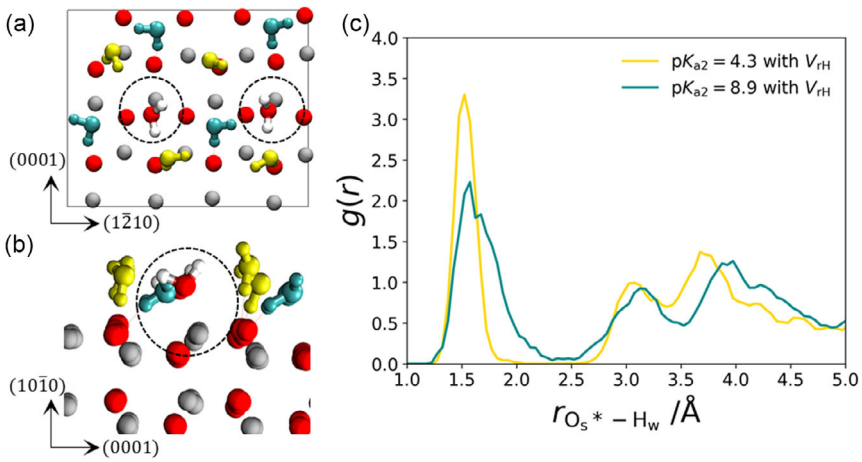

Figure 3. Panel a and b shows the top and side view of the different types of orientations adopted by water molecules on the ZnO$(10\bar{1}0)$ surface when V_{rH} constraints are applied. The two different orientations of water facing the alternate bridged oxygen site (O_s) are represented by colors cyan and yellow. The black dashed circle represents water adsorbed on the terminal zinc site (Zn_sOH_2) used in pK_{a1} calculations. Panel c shows the corresponding RDFs between the bridging oxygen used for pK_{a2} calculations and neighboring hydrogen of water molecules (yellow or cyan).

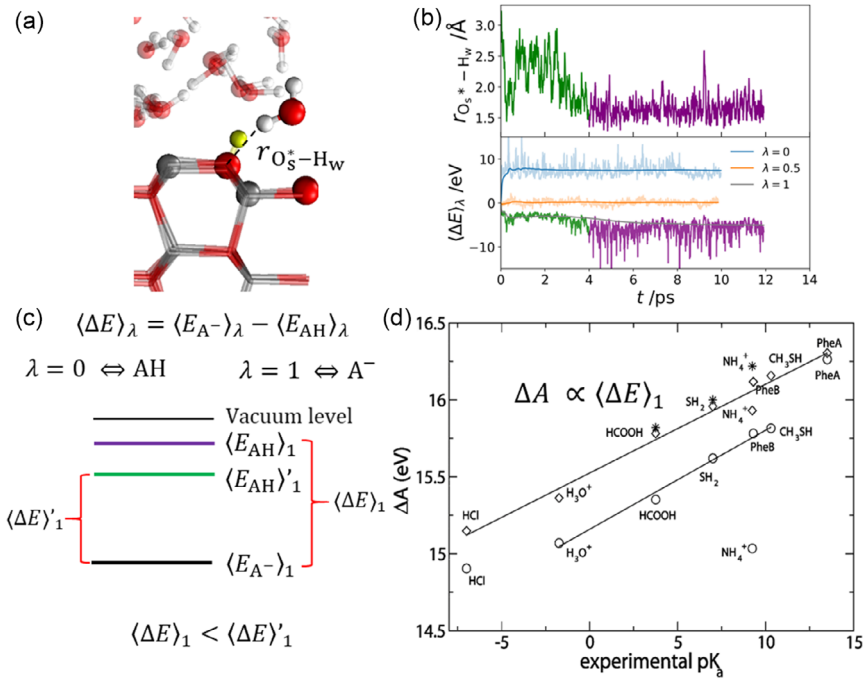

Figure 4. a) A simulation snapshot showing the distance between the bridging oxygen at ZnO(10$\bar{1}$0) and the hydrogen from the surrounding water. b) The time evolution of $\langle\Delta E\rangle_1$ and $r_{O_s^*-H_w}$. c) The energy level diagram for the potential energy of $\lambda = 1$. d) The correlation between ΔA and experimental pK_a. Panel d) was reproduced from ref. [25] with permission from the PCCP Owner Societies.

between the bridging oxygen and the hydrogen of the yellow water is ≈1.525 Å, much shorter than that of the cyan water. Therefore, one would expect that bridging oxygen close to the yellow water is more stabilized by the H-bond and becomes more acidic. Indeed, as shown in Table 2, pK_a of bridging oxygen facing yellow water is 4.3 while that facing cyan water is 8.9. On the other hand, V_{rep} gives consistent results, where the difference between yellow and cyan water is all but disappeared. The latter agrees with the plain DFTMD simulations without V_{rH}, that is, if the water molecules are allowed to freely dissociate (Figure S1, Supporting Information and the corresponding figure caption in the Supporting Information for clarification).

Despite the chemical intuition agreeing with the computed pK_a, it will be desirable to provide insight from the underlying free energy perturbation method. Inspecting Table 1, one notices that $\langle\Delta E\rangle_0$ and $\langle\Delta E\rangle_{0.5}$ are indifferent to the change of $r_{O^*-H_w}$ (see Figure 2). However, $\langle\Delta E\rangle_1$ has a positive correlation with $r_{O^*-H_w}$. This is not a coincidence. Longer $r_{O^*-H_w}$ means more space to insert the proton (by switching back from the dummy atom), a lower probability in overlapping between the inserted proton and the nearby H_w, a lower energy of $\langle E_{AH}\rangle_1$ and a more positive value of $\langle\Delta E\rangle_1$. Since the deprotonation free energy ΔA is proportional to $\langle\Delta E\rangle_1$, this in turn leads to a higher pK_a value. These relationships are summarized in **Figure 4**.

3.3. Repulsive Potential and pK_a of $Zn_2O_sH^+$

By applying the optimized V_{rep} to the ZnO(10$\bar{1}$0)/NaCl sol. system for computing surface pK_a, we found a smaller water dissociation free energy of 0.19 eV, as compared to 0.23 eV for TiO_2(110)/H_2O[13] and 0.32 eV for $BiVO_4$(10)/NaCl sol. systems.[27] However, this value is considerably larger than SnO_2(110)/H_2O system which also shows a high degree of dissociative water adsorption.[14] As a consequence, the PZC turns out to be only mildly basic (Table 2). Thus, one may expect an even smaller $\Delta A_{diss,H_2O}$

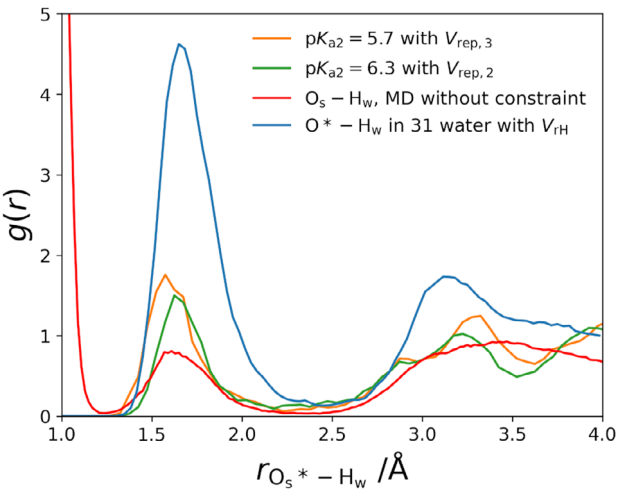

Figure 5. RDF between the bridging oxygen site and the neighboring hydrogen of water molecules is shown. The orange and the green curves correspond to the ZnO(10$\bar{1}$0)/NaCl sol. simulations with $V_{rep,3}$ and $V_{rep,2}$ applied to the system according to Equation 14. The red curve corresponds to the ZnO(10$\bar{1}$0)/NaCl sol. MD simulations run without constraints and represent the RDF between all bridging oxygen sites on the surface and the neighboring hydrogens of water and adsorbed hydroxyl ions. The blue curve corresponds to the reference DFTMD simulation of one OH^- in 31 water molecules, and the RDF between the O atom of OH^- and the neighboring hydrogen of water molecules is shown.

given the high water dissociation percentage reported in the Introduction. This makes us wonder what can be further improved.

One needs to remember that the optimized V_{rep} was obtained for OH^- in liquid water because of the computational feasibility. Although it is justifiable to use OH^- in liquid water as an analog for the surface group of Zn_sOH^- (see Figure S3, Supporting Information), there is no such guarantee for the case of weakly acidic $Zn_2O_sH^+$. Given the insight that a stronger repulsive potential leads to a higher pK_a value, we decided to also apply $V_{rep,2}$ to recompute the pK_a of $Zn_2O_sH^+$. As expected, $V_{rep,2}$ leads to a higher pK_a of $Zn_2O_sH^+$, which is about 6.3. Indeed, $V_{rep,2}$ results in a more positive $\langle \Delta E \rangle_1$ (see Table S2, Supporting Information), agreeing with the scheme shown in Figure 4c,d. The corresponding RDFs between the bridging oxygen and the surrounding H_w of water is shown in **Figure 5**. Combining this result with those listed in Table 2, our best estimation of PZC for the ZnO(10$\bar{1}$0)/NaCl sol. system becomes 7.5 and the corresponding $\Delta A_{diss,H_2O}$ is 0.13 eV.

4. Conclusion

In this study, we have applied DFTMD simulation and free energy perturbation method to compute the surface pK_a of the ZnO(10$\bar{1}$0)/NaCl sol. system.

By reparameterizing the repulsive potential which applies to the surface oxygen group and the surrounding H_w of water, we found that V_{rep} approach provides a consistent description of pK_a of $Zn_2O_sH^+$, which otherwise shows two distinct local solvation environments with the restraining potential V_{rH}.

Our study reveals that a stronger V_{rep} leads to more positive vertical energy gap $\langle \Delta E \rangle_1$ and thereby a higher pK_a value. This insight from the free energy perturbation method agrees with the chemical intuition that a weaker H-bond leads to a stronger base.

Taking this insight, we showed that different V_{rep} are needed to obtain accurate predictions of surface pK_a s for ZnO. For basic oxides, the deprotonated state has a strong tendency to be reprotonated from the surrounding water, which makes the choice of the repulsive potential delicate. Therefore, this point is likely to be general for determining the surface pK_a of basic oxides from DFTMD simulation or its machine learning potential counterpart.

Acknowledgements

This project has received funding from the European Research Council (ERC) under the European Union's Horizon 2020 research and innovation program (grant agreement no. 949012) and the Swedish National Strategic e-Science program eSSENCE. We thank L. Knijff for building up the initial ZnO/NaCl sol. system as well as M. Jia and J. Cheng for helpful discussions on ref. [14]. The simulations were performed on the resources provided by the National Academic Infrastructure for Supercomputing in Sweden (NAISS) at PDC partially funded by the Swedish Research Council through grant agreement no. 2022-06725 and through the project access to the LUMI supercomputer, owned by the EuroHPC Joint Undertaking, hosted by CSC (Finland) and the LUMI consortium.

Conflict of Interest

The authors declare no conflict of interest.

Data Availability Statement

The data that support the findings of this study are available in the supplementary material of this article.

Keywords: solid–liquid interface · solvation · surface acidities · zinc oxides

[1] Y. Wang, M. Muhler, C. Wöll, *Phys. Chem. Chem. Phys.* **2006**, *8*, 1521.
[2] B. Meyer, D. Marx, O. Dulub, U. Diebold, M. Kunat, D. Langenberg, C. Wöll, *Angew. Chem. Int. Ed.* **2004**, *43*, 6641.
[3] D. Raymand, A. C. T. van Duin, M. Baudin, K. Hermansson, *Surf. Sci.* **2008**, *602*, 1020.
[4] N. Kharche, M. S. Hybertsen, J. T. Muckerman, *Phys. Chem. Chem. Phys.* **2014**, *16*, 12057.
[5] G. Tocci, A. Michaelides, *J. Phys. Chem. Lett.* **2014**, *5*, 474.
[6] V. Quaranta, M. Hellström, J. Behler, *J. Phys. Chem. Lett.* **2017**, *8*, 1476.
[7] V. Quaranta, J. Behler, M. Hellström, *J. Phys. Chem. C* **2019**, *123*, 1293.
[8] K. Maeda, K. Domen, *J. Phys. Chem. Lett.* **2010**, *1*, 2655.
[9] S. Heinonen, J.-P. Nikkanen, E. Huttunen-Saarivirta, E. Levänen, *Thin Solid Films* **2017**, *638*, 410.
[10] L. Knijff, M. Jia, C. Zhang, *Encyclopedia of Solid-Liquid Interfaces*, 1st ed., (Eds. K. Wandelt, G. Bussetti), Elsevier, Oxford **2024**, pp. 567–575.
[11] F. Costanzo, M. Sulpizi, R. G. D. Valle, M. Sprik, *J. Chem. Phys.* **2011**, *134*, 244508.
[12] J. Cheng, X. Liu, J. VandeVondele, M. Sulpizi, M. Sprik, *Acc. Chem. Res.* **2014**, *47*, 3522.
[13] J. Cheng, M. Sprik, *J. Chem. Theory Comput.* **2010**, *6*, 880.
[14] M. Jia, C. Zhang, S. J. Cox, M. Sprik, J. Cheng, *J. Chem. Theory Comput.* **2020**, *16*, 6520.
[15] T. D. Kühne, M. Iannuzzi, M. Del Ben, V. V. Rybkin, P. Seewald, F. Stein, T. Laino, R. Z. Khaliullin, O. Schütt, F. Schiffmann, D. Golze, J. Wilhelm, S. Chulkov, M. H. Bani-Hashemian, V. Weber, U. Borštnik, M. Taillefumier, A. S. Jakobovits, A. Lazzaro, H. Pabst, T. Müller, R. Schade, M. Guidon, S. Andermatt, N. Holmberg, G. K. Schenter, A. Hehn, A. Bussy, F. Belleflamme, G. Tabacchi, et al., *J. Chem. Phys.* **2020**, *152*, 194103.
[16] J. VandeVondele, M. Krack, F. Mohamed, M. Parrinello, T. Chassaing, J. Hutter, *Comput. Phys. Commun.* **2005**, *167*, 103.
[17] A. D. Becke, *Phys. Rev. A* **1988**, *38*, 3098.
[18] C. Lee, W. Yang, R. G. Parr, *Phys. Rev. B* **1988**, *37*, 785.
[19] J. P. Perdew, K. Burke, M. Ernzerhof, *Phys. Rev. Lett.* **1996**, *77*, 3865.
[20] J. VandeVondele, J. Hutter, *J. Chem. Phys.* **2007**, *127*, 114105.
[21] S. Grimme, J. Antony, S. Ehrlich, H. Krieg, *J. Chem. Phys.* **2010**, *132*, 154104.
[22] S. Goedecker, M. Teter, J. Hutter, *Phys. Rev. B* **1996**, *54*, 1703.
[23] C. Hartwigsen, S. Goedecker, J. Hutter, *Phys. Rev. B* **1998**, *58*, 3641.
[24] G. Bussi, D. Donadio, M. Parrinello, *J. Chem. Phys.* **2007**, *126*, 014101.
[25] M. Sulpizi, M. Sprik, *Phys. Chem. Chem. Phys.* **2008**, *10*, 5238.
[26] D. Reith, M. Pütz, F. Müller-Plathe, *J. Comput. Chem.* **2003**, *24*, 1624.
[27] M. Jia, J. Wang, Q. Liu, X. Yang, C. Zhang, *J. Chem. Phys.* **2024**, *161*, 104702.

Manuscript received: March 24, 2025
Revised manuscript received: May 22, 2025
Version of record online: June 13, 2025